



A computationally-efficient hierarchical scaling law to predict damage accumulation in composite fibre-bundles



Soraia Pimenta

Department of Mechanical Engineering, South Kensington Campus, Imperial College, London, SW7 2AZ, United Kingdom

ARTICLE INFO

Article history:

Received 28 February 2017

Received in revised form

12 April 2017

Accepted 13 April 2017

Available online 18 April 2017

Keywords:

A. Polymer–matrix composites

B. Fragmentation

B. Stress/strain curves

C. Modelling

C. Probabilistic methods

ABSTRACT

Unidirectional composites under longitudinal tension develop damage through the accumulation and clustering of fibre-breaks, which may lead to catastrophic failure of an entire structure. This paper uses a hierarchical scaling law to predict the kinetics of fibre-breakage and its effect on the stress-strain response of composites under longitudinal tension; due to its analytical formulation based on the statistical analysis of hierarchical fibre-bundles, the scaling law predicts the response of composite bundles up to virtually any size in less than one second. Model predictions for the accumulation and clustering of fibre-breaks are successfully validated against experiments from the literature. These results show that the present model is a much more computationally-efficient alternative to other state-of-the-art models based on Monte-Carlo simulations, without sacrificing the accuracy of predictions when compared against experiments.

© 2017 Elsevier Ltd. All rights reserved.

1. Introduction

The response of UniDirectional Fibre-Reinforced Polymers (UD-FRPs) under longitudinal tension is characterised by the progressive accumulation and clustering of fibre-breaks, in a process which eventually creates a critical cluster of broken fibres that often triggers the unstable failure of the structure [1,2]. This response is governed by (i) the variability of the strength of individual fibres (commonly assumed to follow a Weibull distribution [3], although this has been debated in the literature [4–7]) and (ii) the stress-redistribution near fibre-breaks (controlled by the matrix) [8–11].

These two features have been incorporated in several fibre-bundle models to predict the strength of UD-FRPs and the associated size effects. The earlier models [12–15] were analytical, and could predict the average or the full strength distribution of either small [13] or asymptotically-large bundles [12,14,15]. Further analytical developments have studied the effect of different load-sharing schemes, but required parameters fitted through computational simulations [5,16–19]. Most analytical models have not been validated experimentally [12–14,16–19], apart from isolated comparisons on the mean strength only [5,15] (with models overpredicting experiments by at least 10%).

More recently, the increase in computational power enabled

several researchers to propose Monte-Carlo simulations for the tensile failure process in UD-FRPs [5,16–30]. These models aim to represent stress fields near single fibre-breaks accurately, although most assume regular packing [5,17–25,27,30]; many models [16,18,25,26] also neglect the increase in the stress-recovery length near broken clusters, which was shown to overestimate bundle strength [30]; moreover, all models [5,16–27,30] consider simplified matrix constitutive laws (e.g. neglecting progressive matrix fracture), neglect dynamic stress concentrations, and assume perfectly-aligned fibres (the only exceptions [28,29] considered very small representative volume elements). In addition, simulation results are often not compared against experiments [16–20,26,28,29], and when compared they tend to overpredict the average strength of composites [5,21,22,24,25]; they also significantly underpredict the variability of strength distributions [25], and underpredict (or fail to predict) size-effects for increasing filament counts in bundles [22,26]. This shows that direct numerical simulations which aim to capture “second-order effects” are not only computationally very expensive, but they do not yet capture all relevant mechanics of composite fibre-bundles under longitudinal tension, as it has been recognised in a recent review [31].

Pimenta and Pinho [32] proposed an analytical *hierarchical scaling law* to predict the full strength distributions of composite fibre-bundles of any size. This model considers a perfectly-plastic shear-lag stress transfer (neglecting matrix strain-hardening and fibre-matrix debonding) in the neighbourhood of fibre-breaks,

E-mail address: soraia.pimenta@imperial.ac.uk.

Nomenclature	
<i>Uppercase variables</i>	
A	cross-sectional area (based on fibres only)
C	perimeter of the shear-lag boundary
\mathcal{C}_K	constant for survivability under linear stress —concentrations
E	Young's modulus
N	number of breaks/clusters
F	failure probability (strength distribution)
S	survival probability
V	volume
X	longitudinal tensile strength
<i>Lowercase variables</i>	
e	stress-strain non-linearity
i	bundle level
j	sub-bundle/cluster level
k	stress concentrations factor
l	length
m	Weibull shape parameter
n	number of fibres in bundle/cluster
ϵ	longitudinal strain
ϕ	diameter
ρ	density (over volume of fibres)
s	interfibre spacing
σ	longitudinal stress
τ	shear (yield) stress
ξ	strain factor under linear stress-concentrations
<i>Superscripts</i>	
f	fibre
$[i]$	bundle level
∞	remote
<i>Subscripts</i>	
0	Weibull scale parameter
break	individual fibre-breaks
c	control length
clust	cluster of broken-fibres
crit	critical value
e	effective recovery length
\mathcal{K}	one sub-bundle fails and the other survives
K	linear stress concentrations state
\max	largest value
s	specimen
SL	shear-lag
U	uniform stress state
\mathcal{W}	both sub-bundles survive
<i>Operators (on variable χ)</i>	
$\bar{\chi}$	average value
$\hat{\chi}$	expected value
$f(\chi; \alpha)$	function of χ with parameter α

and analyses the propagation of failure using a number of broken fibres in a geometric progression with ratio $c = 2$ (see Fig. 1a). This makes the model computationally efficient, predicting full strength distributions and size effects in bundles up to a million fibres in less than one second. Moreover, this model was validated against experiments from the literature [22,33,34], using only physically-based inputs with no fitting parameters, across the full range of scales. This model has also been successfully used to predict the translaminar fracture toughness of unidirectional FRPs under longitudinal tension [35], and to engineer the fracture surface and promote toughening of FRPs [36].

Another challenge faced by models for the longitudinal tensile failure of UD-FRPs is the prediction of damage accumulation and the kinetics of fibre-breakage. This has been studied experimentally by Aroush et al. [1] using quartz-epoxy bundles embedded in a large matrix ring. More recently, Scott et al. [2] measured the kinetics of fibre-breakage in carbon/epoxy FRPs with a fibre volume fraction of 60%, using high-resolution in-situ micro-Computed Tomography (micro-CT); further analysis [31]

revealed modest levels of damage and small broken-clusters only (with up to 14 fibres), and noticed that 70% of clusters consisted of perfectly co-planar (rather than diffuse or staggered) fibre-breaks.

Very few models [31,37] have compared their predictions against these detailed experiments; these models successfully captured qualitative features and trends, but they overpredicted the strength of the material and the density of fibre-breaks at failure [31,37], and also predicted more diffuse fibre-breakage patterns than those observed experimentally [31]. Although other models in the literature [18–25] have not been directly compared against these detailed experiments, they still present qualitatively similar discrepancies, by predicting large levels of damage just before final failure [18–25], and the formation of diffuse clusters [17,20,22–25] with more than 50 fibre-breaks before final failure [17,21,22,25]. Consequently, the experiments from Scott et al. [2] are still an open and unsolved challenge for micromechanical models for the longitudinal tensile failure of composites.

Models for the longitudinal tensile strength of FRPs can also be used to predict the stiffness reduction due to the accumulation of

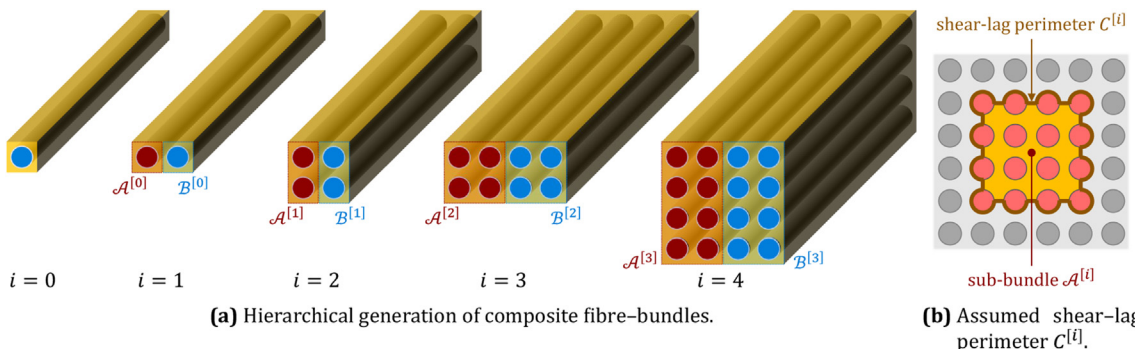


Fig. 1. Geometry of hierarchical composite fibre-bundles.

fibre-breaks and, consequently, the full stress-strain curves of composites. However, analytical models in the literature [12–19] have not predicted full tensile stress-strain curves for UD-FRPs. Moreover, Monte-Carlo simulations predict a considerable amount of non-linearity for UD-FRPs under longitudinal tension [5,20,22,23,25,27]; this is contradicted by experimental evidence, which shows seemingly linear-elastic responses up to brittle failure [38].

The ability to predict the accumulation of fibre-breaks and their effect on the linearity of the macroscopic tensile response of UD-FRPs can be used to develop stronger and more damage-tolerant materials, to develop monitoring strategies, and to define acceptable levels of damage in FRP structures. In this context, this paper develops the hierarchical scaling law for the strength of composites proposed by Pimenta and Pinho [32] further, in order to predict the evolution of damage in UD-FRPs, including the accumulation and clustering of fibre-breaks and their effect on the material's stress-strain curve. Due to the analytical formulation of the hierarchical scaling law, the accumulation of damage in a composite bundle is *not* a by-product of a simulation to predict its strength (as it is for instance in Monte-Carlo simulations), which makes the new developments detailed in this paper non-trivial and original.

Section 2 presents the development and implementation of the model: Subsections 2.1–2.2 summarise the previously-developed [32] scaling law for predicting strength distributions, while the original analytical developments for calculating the strains and fibre-breakage are described in Subsections 2.3–2.5. Original results are explored and validated against Scott et al.'s experiments [2] in Section 3. Section 4 discusses the insight provided by the model and where it stands in the existing literature, and the main conclusions are summarised in Section 5.

2. Model development

2.1. Model assumptions

The model proposed in this paper uses a hierarchical scaling law for the strength distribution of composite fibre-bundles based on the following assumptions:

I. The analysis considers hierarchical fibre-bundles (Fig. 1), which are generated by pairing two individual fibres (level-[0], represented by $\mathcal{A}^{[0]}$ and $\mathcal{B}^{[0]}$) into a level-[1] bundle, and then recursively grouping two level-[i] bundles (represented by $\mathcal{A}^{[i]}$ and $\mathcal{B}^{[i]}$) into one level-[$i+1$] bundle. The number of fibres ($n^{[i]}$) in a level-[i] bundle is therefore

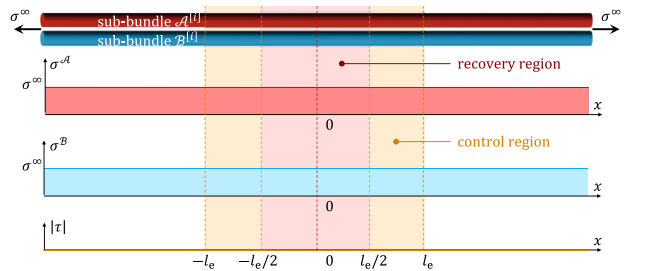
$$n^{[i]} = 2^i \Leftrightarrow i = \log_2 n^{[i]}. \quad (1)$$

II. The fibres (superscript "f" or [0]) resist longitudinal stresses only. Their strength under an uniform stress field (σ^∞ applied remotely) follows a Weibull distribution with shape parameter m and scale parameter σ_0^f [3], measured at the reference length l_0 . The single-fibre strength distribution and its survival probability (respectively $F_U^{[0]}(\sigma^\infty)$ and $S_U^{[0]}(\sigma^\infty)$) can be scaled to any length l through the Weakest Link Theory (WLT), according to

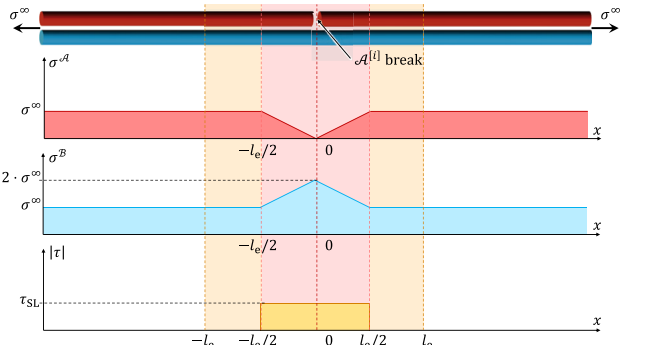
$$\begin{aligned} F_U^{[0]}(\sigma^\infty; l) &= 1 - \exp\left[-\frac{l}{l_0} \cdot \left(\frac{\sigma^\infty}{\sigma_0^f}\right)^m\right] \quad \text{and} \\ S_U^{[0]}(\sigma^\infty; l) &= \exp\left[-\frac{l}{l_0} \cdot \left(\frac{\sigma^\infty}{\sigma_0^f}\right)^m\right]. \end{aligned} \quad (2)$$

III. The fibres are embedded in a soft matrix (or fibre-matrix interface) that redistributes stresses in the neighbourhood of fibre-breaks according to a perfectly-plastic shear-lag model with yield stress τ_{SL} . The shear-lag stress τ_{SL} , together with the effective perimeter and area of the fibre, govern the rate and length for stress-recovery in broken fibres and also, through equilibrium, the stress-concentrations in surviving fibres (see Fig. 2 and Equation 4 in Section 2.2).

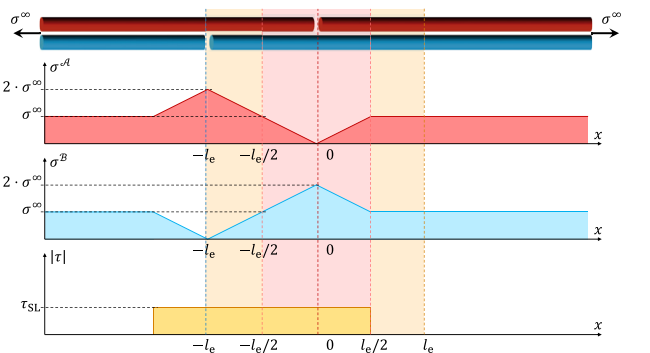
IV. Failure propagates hierarchically in a self-similar way. This is based on (i) micro-CT experiments showing that 70% of the clusters are formed by a group of perfectly co-planar fibre-breaks which occur simultaneously [31], and (ii) self-similar motifs observed on the fracture surfaces of UD-FRPs (with individual fibres protruding from small bundles, which are themselves pulled-out from larger bundles) [35,39,40]. This suggests that failure can be analysed at a range of discrete scales (i.e. *hierarchically*), and that



(a) Both level-[i] sub-bundles survive (consequently, the level-[$i+1$] bundle survives).



(b) Level-[i] sub-bundle $\mathcal{A}^{[i]}$ fails and the neighbouring sub-bundle $\mathcal{B}^{[i]}$ survives (consequently, the level-[$i+1$] bundle survives).



(c) Both level-[i] sub-bundles fail within the control length $l_c = 2 \cdot l_e$ (consequently, the level-[$i+1$] bundle fails).

Fig. 2. Scenarios for survival and failure of a level-[$i+1$] bundle. The stress fields represented assume (without loss of generality) that sub-bundle $\mathcal{A}^{[i]}$ is weaker than sub-bundle $\mathcal{B}^{[i]}$, and weakest at $x = 0$. The level-[i] recovery length is represented as $l_e \equiv l_e^{[i]}(\sigma^\infty)$ for simplicity.

failure of those different scales is governed by the same mechanisms (*self-similarity*). For these reasons, this model analyses bundle failure in two steps:

- (1) derivation of the mathematical description of the failure process in a level-[1] bundle (composed of two level-[0] fibres);
- (2) extrapolation of the mathematical description derived in Step (1) to describe the failure process in a generic level-[i+1] bundle (composed of two level-[i] sub-bundles).

2.2. Hierarchical scaling law for strength distributions

Based on the assumptions described in Section 2.1, Pimenta and Pinho [32] derived the following hierarchical expression for the survival probability of a level-[i+1] bundle under a remote stress σ^∞ :

$$S_{U,c}^{[i+1]}(\sigma^\infty) = S_{U,e}^{[i]}(\sigma^\infty)^4 + 2 \cdot \left[1 - S_{U,e}^{[i]}(\sigma^\infty)^2 \right] \cdot S_{U,e}^{[i]}(\sigma^\infty) \cdot S_{K,e}^{[i]}(\sigma^\infty). \quad (3)$$

In Equation 3, $S_{U,e}^{[i]}(\sigma^\infty)$ is the survival probability of a level-[i] sub-bundle under uniform stresses (with increasing magnitude σ^∞), and $S_{K,e}^{[i]}(\sigma^\infty)$ is its survival probability under linear stress concentrations (with the profile shown in Fig. 2b for sub-bundle $\mathcal{B}^{[i]}$ in $|x| \leq l_e^{[i]}/2$). All longitudinal stresses throughout this paper are normalised by the cross-section of the fibres only.

The level-[i] survival probabilities in Equation 3 are calculated at the level-[i] shear-lag recovery length $l_e^{[i]}$ (subscript “e”), and the resulting level-[i+1] survival probability is calculated at the level-[i+1] control length $l_c^{[i+1]}$ (subscript “c”); these are defined through shear-lag (see Fig. 2) as

$$l_e^{[i]}(\sigma^\infty) = 2 \cdot \frac{A^{[i]}}{C^{[i]} \cdot \tau_{SL}} \cdot \sigma^\infty \quad \text{and} \quad l_c^{[i+1]}(\sigma^\infty) = 2 \cdot l_e^{[i]}(\sigma^\infty), \quad (4)$$

where the cross-sectional area $A^{[i]}$ and shear-lag perimeter $C^{[i]}$ of the level-[i] sub-bundle (identified in Fig. 1b) can be found in Appendix A. The control length $l_c^{[i+1]}$ defined in Equation 4 is the shortest statistically independent partition of a bundle, as shown in Fig. 2b: if sub-bundle $\mathcal{B}^{[i]}$ fails outside the control region, the level-[i+1] bundle can still resist an increase in remote stress because the matrix/interface is not fully yielded in between the two level-[i] breaks. It is noted that Equation 3 assumes that each level-[i] sub-bundle can fail only once in the control region [32].

The stress-concentration profile in Fig. 2b is calculated from equilibrium of sub-bundles $\mathcal{A}^{[i]}$ and $\mathcal{B}^{[i]}$, which yields a maximum stress concentration factor $k = 2$, for any bundle and broken-cluster size. While this overestimates stress concentration factors predicted through FE analyses [8,11,24,30,41] and neglects the dependence of stress concentrations with size of broken-cluster [30], it is a direct consequence of the hierarchical and self-similar failure propagation mode (see point IV in the previous section), and it can account indirectly for many real effects — e.g. dynamic stress concentrations, fibre misalignments, and effect of large broken clusters — which are neglected in many Monte-Carlo simulation models [5,16–27]. Moreover, the present approach accounts for the actually decreasing stress concentrations along the fibre-direction (i.e. within the recovery length) as predicted by shear-lag, contrarily to other analytical models [5,12–19] which consider uniform stress

concentrations along the entire recovery length.

The level-[i] strength distributions ($S_{U,e}^{[i]}(\sigma^\infty)$ and $S_{K,e}^{[i]}(\sigma^\infty)$) used in the scaling law (Equation 3) can be calculated (see Appendix B) directly from $S_{U,c}^{[i]}(\sigma^\infty)$. Consequently, Equation 3 relates the survival probabilities of bundles of consecutive levels (i and $i+1$), and it can thus be used recursively to scale the strength distribution of a single-fibre (level-[0]) up to a bundle of any level [$i+1$], as detailed elsewhere [32]. The novelty of the present paper consists on using the survival probabilities defined in Equation 3 to predict the accumulation of fibre breaks and the corresponding non-linearity in the tensile response of composite fibre-bundles, as described in Sections 2.3–2.5.

2.3. Scenarios for survival and failure of a bundle

The scaling law in Equation 3 considers three possible scenarios for a level-[i+1] bundle under a uniform remote stress σ^∞ (see Fig. 2):

- (a) The level-[i+1] bundle survives with no level-[i] breaks. In this case, both level-[i] sub-bundles $\mathcal{A}^{[i]}$ and $\mathcal{B}^{[i]}$ (each with two segments of length $l_e^{[i]}$) withstand the uniform stress σ^∞ (as shown in Fig. 2a) within the level-[i+1] control length. The probability of this scenario (subscript \mathcal{U}) corresponds to the first term in Equation 3 [32]:

$$S_{\mathcal{U}}^{[i+1]}(\sigma^\infty) \stackrel{\text{def}}{=} S_{U,e}^{[i]}(\sigma^\infty)^4; \quad (5a)$$

- (b) The level-[i+1] bundle survives with one level-[i] break. In this case, the level-[i] sub-bundle $\mathcal{A}^{[i]}$ (with two segments of length $l_e^{[i]}$) fails under the uniform stress σ^∞ , and its neighbouring level-[i] sub-bundle $\mathcal{B}^{[i]}$ withstands the resulting stress field (with one segment of length $l_e^{[i]}$ under linear stress concentrations, and another under uniform stresses, as shown in Fig. 2b). The probability of this scenario (subscript \mathcal{K}) corresponds to the second term in Equation 3 [32]:

$$S_{\mathcal{K}}^{[i+1]}(\sigma^\infty) \stackrel{\text{def}}{=} 2 \cdot \left[1 - S_{U,e}^{[i]}(\sigma^\infty)^2 \right] \cdot S_{U,e}^{[i]}(\sigma^\infty) \cdot S_{K,e}^{[i]}(\sigma^\infty); \quad (5b)$$

- (c) The level-[i+1] bundle fails. In this case, both level-[i] sub-bundles ($\mathcal{A}^{[i]}$ and $\mathcal{B}^{[i]}$) fail at a sufficiently small distance so that the matrix in between the broken sections yields completely (as shown in Fig. 2c). The probability of this scenario is given by the complement of Equation 3 [32]:

$$F_{U,c}^{[i+1]}(\sigma^\infty) = 1 - S_{U,c}^{[i+1]}(\sigma^\infty) = 1 - \left[S_{\mathcal{U}}^{[i+1]}(\sigma^\infty) + S_{\mathcal{K}}^{[i+1]}(\sigma^\infty) \right]. \quad (5c)$$

These three scenarios for a level-[i+1] bundle will be used in Sections 2.4 and 2.5 to calculate the expected non-linear stress-strain response and the accumulation of fibre-breaks in a bundle.

2.4. Non-linear stress-strain curves in composite fibre-bundles

2.4.1. Scenario (a): both level-[i] sub-bundles survive

Consider a level-[i+1] bundle in Scenario (a) as described in Section 2.3 and represented in Fig. 2a, i.e. with both level-[i] sub-bundles surviving the remote stress σ^∞ within the control length:

- For $i = 0$ (level-[1] bundle), the sub-bundles are individual fibres, assumed to be linear-elastic with Young's modulus E^f . In this scenario with no fibre-breaks, the strain of the level-[1] bundle averaged within $l_c^{[1]}$ (represented by $\bar{\varepsilon}_c$) is

$$\begin{aligned}\bar{\varepsilon}_{\mathcal{U}}^{[1]}(\sigma^\infty) &= \bar{\varepsilon}_c^{\mathcal{A}^{[0]}}(\sigma^\infty) = \bar{\varepsilon}_c^{\mathcal{B}^{[0]}}(\sigma^\infty) = \bar{\varepsilon}_c^{[0]}(\sigma^\infty), \text{ with} \\ \bar{\varepsilon}_c^{[0]}(\sigma^\infty) &\stackrel{\text{def}}{=} \frac{\sigma^\infty}{E^f},\end{aligned}\quad (6a)$$

where the deformation of fibres $\mathcal{A}^{[0]}$ and $\mathcal{B}^{[0]}$ is simply given by Hooke's law.

- For $i \geq 1$, compatibility of the overall strains between the level-[$i+1$] bundle and its sub-bundles $\mathcal{A}^{[i]}$ and $\mathcal{B}^{[i]}$ still requires that

$$\begin{aligned}\bar{\varepsilon}_{\mathcal{U}}^{[i+1]}(\sigma^\infty) &= \bar{\varepsilon}_c^{\mathcal{A}^{[i]}}(\sigma^\infty) = \bar{\varepsilon}_c^{\mathcal{B}^{[i]}}(\sigma^\infty) = \bar{\varepsilon}_c^{[i]}(\sigma^\infty), \text{ with} \\ \bar{\varepsilon}_c^{[i]}(\sigma^\infty) &\stackrel{\text{def}}{=} \frac{\sigma^\infty}{\hat{E}^{[i]}(\sigma^\infty)}.\end{aligned}\quad (6b)$$

In this case, the expected stiffness of the level-[i] sub-bundle at a given remote stress (represented by $\hat{E}^{[i]}(\sigma^\infty)$) may be smaller than that of the single-fibre (E^f). This is because each surviving level-[i] sub-bundle might itself contain fibre-breaks (either individually dispersed or grouped in clusters of level-[$i-1$] or lower); these breaks are not sufficient to completely fail the level-[i] bundle, but they will increase its local compliance — hence $\bar{\varepsilon}_{\mathcal{U}}^{[i+1]}(\sigma^\infty) \geq \sigma^\infty/E^f$.

2.4.2. Scenario (b): one level-[i] sub-bundle fails, and the other survives

Consider now a level-[$i+1$] bundle in Scenario (b), as described in Section 2.3 and represented in Fig. 2b, i.e. with sub-bundle $\mathcal{A}^{[i]}$ failing and sub-bundle $\mathcal{B}^{[i]}$ surviving. In this case, the strain of the level-[$i+1$] bundle averaged in the control length $l_c^{[i+1]}$ will be controlled by the surviving sub-bundle $\mathcal{B}^{[i]}$, i.e.

$$\bar{\varepsilon}_{\mathcal{U}}^{[i+1]}(\sigma^\infty) = \bar{\varepsilon}_c^{\mathcal{B}^{[i]}}(\sigma^\infty) = \frac{1}{2 \cdot l_e^{[i]}} \cdot \int_{x=-l_e^{[i]}}^{l_e^{[i]}} \varepsilon_{\mathcal{B}^{[i]}}(x; \sigma^\infty) dx. \quad (7a)$$

- For $i = 0$ (level-[1] bundle), the average strain of fibre $\mathcal{B}^{[0]}$ can be calculated directly from integration of the linear-elastic strains within the control length ($l_c^{[i+1]} = 2 \cdot l_e^{[i]}$), and

$$\begin{aligned}\bar{\varepsilon}_{\mathcal{U}}^{[1]}(\sigma^\infty) &\stackrel{\text{def}}{=} \frac{1}{2 \cdot l_e^{[0]}} \cdot \int_{x=-l_e^{[0]}}^{l_e^{[0]}} \frac{\sigma_{\mathcal{B}^{[0]}}(x; \sigma^\infty)}{E^f} dx = \frac{\sigma^\infty}{E^f} \cdot \left(1 + \frac{k-1}{4}\right) \\ &= \bar{\varepsilon}_c^{[0]}(\sigma^\infty) \cdot \left(1 + \frac{k-1}{4}\right).\end{aligned}\quad (7b)$$

- For $i \geq 1$, the compatibility imposed in Equation 7a still applies. However, in this case the surviving sub-bundle $\mathcal{B}^{[i]}$ may contain fibre-breaks, in which case it is no longer linear-elastic. Nevertheless, assuming that the local stiffness of sub-bundle $\mathcal{B}^{[i]}$ under the actual stress field (represented as

$E^{[i]}(\sigma^{\mathcal{B}^{[i]}})$) can be approximated by its expected stiffness under the uniform remote stress (already introduced in Equation 6b as $\hat{E}^{[i]}(\sigma^\infty)$), Equation 7b can be extrapolated to any bundle level as

$$\begin{aligned}\bar{\varepsilon}_{\mathcal{U}}^{[i+1]}(\sigma^\infty) &\stackrel{\text{def}}{=} \frac{1}{2 \cdot l_e^{[i]}} \cdot \int_{x=-l_e^{[i]}}^{l_e^{[i]}} \frac{\sigma_{\mathcal{B}^{[i]}}(x; \sigma^\infty)}{E^{[i]}(\sigma^{\mathcal{B}^{[i]}})} dx \approx \frac{\sigma^\infty}{\hat{E}^{[i]}(\sigma^\infty)} \cdot \left(1 + \frac{k-1}{4}\right) \\ &= \bar{\varepsilon}_c^{[i]}(\sigma^\infty) \cdot \left(1 + \frac{k-1}{4}\right).\end{aligned}\quad (7c)$$

2.4.3. Hierarchical scaling law for non-linear stress-strain response

Equations 6 and 7 define the level-[$i+1$] strains averaged in the control length for Scenarios (a) and (b), which occur with the probabilities in Equations 5a–5b respectively. Consequently, the expected strain (represented as $\hat{\varepsilon}$) of a surviving level-[$i+1$] bundle can be related to that of a surviving level-[i] sub-bundle by

$$\begin{aligned}\hat{\varepsilon}^{[i+1]}(\sigma^\infty) &\stackrel{\text{def}}{=} \frac{1}{S_{U,c}^{[i+1]}(\sigma^\infty)} \cdot [S_{\mathcal{U}}^{[i+1]}(\sigma^\infty) \cdot \bar{\varepsilon}_{\mathcal{U}}^{[i+1]}(\sigma^\infty) \\ &\quad + S_{\mathcal{K}}^{[i+1]}(\sigma^\infty) \cdot \bar{\varepsilon}_{\mathcal{K}}^{[i+1]}(\sigma^\infty)],\end{aligned}\quad (8a)$$

where the factor $1/S_{U,c}^{[i+1]}$ (defined in Equation 3) represents the conditional probability associated with the fact that the level-[$i+1$] bundle survives σ^∞ . If a level-[$i+1$] bundle ($\mathcal{A}^{[i+1]}$ hereafter) fails under σ^∞ (with probability calculated in Equation 5c), its deformation will be either (i) undetermined if $\mathcal{A}^{[i+1]}$ is isolated, or (ii) controlled by its surviving neighbour $\mathcal{B}^{[i+1]}$ if $\mathcal{A}^{[i+1]}$ is embedded in a level-[$i+2$] bundle (through the compatibility imposed in Equation 7a). Using the average strains for the two survival scenarios derived in Equations 6 and 7, Equation 8a can be simplified to

$$\hat{\varepsilon}^{[i+1]}(\sigma^\infty) \stackrel{\text{def}}{=} \left[\frac{S_{\mathcal{U}}^{[i+1]}(\sigma^\infty)}{S_{U,c}^{[i+1]}(\sigma^\infty)} + \left(1 + \frac{k-1}{4}\right) \cdot \frac{S_{\mathcal{K}}^{[i+1]}(\sigma^\infty)}{S_{U,c}^{[i+1]}(\sigma^\infty)} \right] \cdot \bar{\varepsilon}^{[i]}(\sigma^\infty). \quad (8b)$$

Equation 8b can be used recursively to hierarchically scale the strains from the linear-elastic single-fibres (level-[0]) to those in a bundle of any level [$i+1$]. Re-arranging Equation 8b knowing that $S_{\mathcal{U}}^{[i+1]}(\sigma^\infty) = S_{U,c}^{[i+1]}(\sigma^\infty) - S_{\mathcal{K}}^{[i+1]}(\sigma^\infty)$ (as defined in Equation 3), this scaling law for the expected non-linear stress-strain response of bundles can be written as

$$\begin{aligned}\hat{\varepsilon}^{[i+1]}(\sigma^\infty) &= e^{[i+1]}(\sigma^\infty) \cdot \hat{\varepsilon}^{[i]}(\sigma^\infty), \\ \text{where } e^{[i+1]}(\sigma^\infty) &\stackrel{\text{def}}{=} 1 + (\xi - 1) \cdot \frac{S_{\mathcal{K}}^{[i+1]}(\sigma^\infty)}{S_{U,c}^{[i+1]}(\sigma^\infty)} \quad \text{and} \quad \xi \stackrel{\text{def}}{=} 1 + \frac{k-1}{4}.\end{aligned}\quad (9)$$

2.5. Accumulation and clustering of fibre-breaks

2.5.1. Density of broken clusters

The strategy used in Section 2.4 to calculate the expected non-linear response in composite fibre-bundles can also be applied to the accumulation of fibre-breaks and broken-clusters. Consider once again the three possible scenarios for a level-[$i+1$] bundle

described in Section 2.3 and in Fig. 2:

- (a) Both level-[i] sub-bundles $\mathcal{A}^{[i]}$ and $\mathcal{B}^{[i]}$ survive (with associated probability $S_{\mathcal{H}}^{[i+1]}(\sigma^\infty)$ given by Equation 5a). In this case, there is no level-[i] broken cluster in the control length of the level-[i+1] bundle (although there may be lower-level clusters (of level $j \leq i-1$) in sub-bundles $\mathcal{A}^{[i]}$ and $\mathcal{B}^{[i]}$);
- (b) One level-[i] sub-bundle fails, and the other survives (with associated probability $S_{\mathcal{H}}^{[i+1]}(\sigma^\infty)$ given by Equation 5b). In this case, there will be one level-[i] broken-cluster in the level-[i+1] bundle, within the control length $l_c^{[i+1]}$. Consequently, the probability $S_{\mathcal{H}}^{[i+1]}(\sigma^\infty)$ will be used to calculate the density of level-[i] clusters (in Equation 10);
- (c) Both level-[i] sub-bundles fail (with associated probability $F_{U,c}^{[i+1]}(\sigma^\infty)$ given by Equation 5c). In this case, there will be no level-[i] broken cluster, as the two breaks in the sub-bundles would be considered clustered into one larger break of level-[$j \geq i+1$].

From these three possible scenarios, the probability of having a level-[i] broken-cluster is $S_{\mathcal{H}}^{[i+1]}(\sigma^\infty)$; this is associated with the control length $l_c^{[i+1]}$ of a level-[i+1] bundle (in which each sub-bundle $\mathcal{A}^{[i]}$ and $\mathcal{B}^{[i]}$ can only fail once). The expected density ($\hat{\rho}_{\text{clust}}^{[i]}$) of level-[i] broken-clusters in a level-[i+1] bundle (normalised by the volume $V_c^{[i+1]}(\sigma^\infty)$ of the level-[i+1] control region, as shown in Fig. 2) is therefore

$$\hat{\rho}_{\text{clust}}^{[i]}(\sigma^\infty) \stackrel{\text{def.}}{=} \frac{S_{\mathcal{H}}^{[i+1]}(\sigma^\infty)}{V_c^{[i+1]}(\sigma^\infty)}, \quad \text{where } V_c^{[i+1]}(\sigma^\infty) \stackrel{\text{def.}}{=} A^{[i+1]} \cdot l_c^{[i+1]}(\sigma^\infty). \quad (10)$$

It is noted that, since all stresses are normalised by the cross-section of fibres only (given by $A^{[i]}$ for a given level), the control volume $V_c^{[i+1]}$ does not include the volume of the matrix.

2.5.2. Total density and total number of fibre breaks

Due to the assumption of hierarchical propagation of fibre-breaks in discrete powers of 2 (see Fig. 1a), the total density of fibre-breaks in a level-[$i > 0$] bundle may contain contributions from broken clusters of the following levels:

- $j = 0$. Each occurrence of a level-[0] cluster will contribute with exactly one single fibre-break ($n^{[0]} = 1$), which is (by definition) not included in any cluster of a higher level [$j' \geq 1$] (as the density $\hat{\rho}_{\text{clust}}^{[0]}$ calculated in Equation 11 assumes Scenario (b) in Section 2.3 and Fig. 2b);
- $1 \leq j < i-1$. As in the previous point, each occurrence of a level-[j] cluster will contribute with exactly $n^{[j]} = 2^j$ fibre-breaks, which are (by definition) not included in any cluster of a higher level [$j' \geq j+1$]. A level-[j] cluster may be interacting with lower-level clusters (of level [$j' \leq j-1$]), but the contribution of the latter to the total density of fibre-breaks is accounted for in the respective (lower) level-[j'];
- $j = i-1$, which is the largest cluster that can be formed in a level-[i] bundle. In this case, one-half of the bundle is broken ($\mathcal{A}^{[i]}$ in Fig. 2b), contributing with $n^{[i-1]} = 2^{i-1}$ fibre-breaks; the other-half ($\mathcal{B}^{[i]}$ in Fig. 2b) may have smaller broken-clusters (of level [$0 \leq j' < i-1$]), but it still has at least one individual fibre resisting the load and the stress concentrations.

Following from this analysis, and accounting for the

contribution of all levels $j < i$, the expected density of fibre-breaks in the level-[i] bundle can be calculated as

$$\begin{aligned} \hat{\rho}_{\text{breaks}}^{[i]}(\sigma^\infty) &\stackrel{\text{def.}}{=} \sum_{j=0}^{i-1} n^{[j]} \cdot \hat{\rho}_{\text{clust}}^{[j]}(\sigma^\infty) \\ &\Leftrightarrow \boxed{\hat{\rho}_{\text{breaks}}^{[i]}(\sigma^\infty) = \hat{\rho}_{\text{breaks}}^{[i-1]}(\sigma^\infty) + n^{[i-1]} \cdot \hat{\rho}_{\text{clust}}^{[i-1]}(\sigma^\infty)}. \end{aligned} \quad (11)$$

Equation 11 provides a recursive hierarchical scaling law for the accumulation of fibre-breaks. This assumes explicitly that the density of small broken-clusters (including individual fibre-breaks) at a given applied stress is not affected by the overall size of a large structure.

On the contrary, the total number of broken fibres must be directly affected by the overall size of the structure. Considering a level-[i] composite fibre-bundle of length l_s and with a cross-sectional area of fibres $A^{[i]}$, the expected number of fibre-breaks can be calculated as

$$\hat{N}_{\text{breaks}}^{[i]}(\sigma^\infty) \stackrel{\text{def.}}{=} \hat{\rho}_{\text{breaks}}^{[i]}(\sigma^\infty) \cdot V_s^{[i]}, \quad \text{where } V_s^{[i]} = A^{[i]} \cdot l_s. \quad (12)$$

2.5.3. Number of broken clusters and largest cluster in a bundle

A level-[i] bundle may have broken-clusters ranging from level-[0] (i.e. individual fibre-breaks) up to level-[i-1] (i.e. large clusters of 2^{i-1} broken fibres). The expected number of level-[$j < i$] clusters of broken-fibres in a composite fibre-bundle of level-[i] and volume $V_s^{[i]}$ is

$$\hat{N}_{\text{clust}}^{[j|i]}(\sigma^\infty) \stackrel{\text{def.}}{=} \hat{\rho}_{\text{clust}}^{[j]}(\sigma^\infty) \cdot V_s^{[i]}, \quad \forall j \in \{0, \dots, i-1\}. \quad (13)$$

From the expected number of level-[j] clusters formed in a level-[i] bundle defined in Equation 13, it is then considered that, at a given remote stress σ^∞ , the largest broken-cluster in a level-[i] bundle is of level $\hat{j}_{\max}^{[i]}$ if there is at least one expected broken-cluster of that level, and none of the levels above. Since, in the model, the expected number of broken clusters ($\hat{N}_{\text{clust}}^{[j|i]}$) is a continuous variable on σ^∞ , the level of the largest broken-cluster ($\hat{j}_{\max}^{[i]}$) is mathematically calculated by imposing that the expected number of level- $\hat{j}_{\max}^{[i]}$ broken clusters ($\hat{N}_{\text{clust}}^{[\hat{j}_{\max}^{[i]}]}$) is above a threshold $N_{\text{thresh}} = 0.5$:

$$\hat{j}_{\max}^{[i]}(\sigma^\infty) \stackrel{\text{def.}}{=} \max \left\{ j \in \{0, \dots, i-1\} : \hat{N}_{\text{clust}}^{[j|i]}(\sigma^\infty) \geq N_{\text{thresh}} \right\}. \quad (14)$$

Choosing a threshold (N_{thresh}) to detect the formation of a broken-cluster of level-[j] is required because the expected number of clusters predicted by the model is a continuous variable ($\hat{N}_{\text{clust}}^{[j|i]}(\sigma^\infty) \in \mathbb{R}^+$); the choice of $N_{\text{thresh}} = 0.5$ seems to be the most obvious one, as it identifies the applied stress σ^∞ at which the expected number of [j]-clusters is closer to 1 than to zero. Choosing other threshold value within the (also reasonable) interval $0.5 \leq N_{\text{thresh}} \leq 1.0$ would not significantly affect the evolution of the largest broken-cluster $\hat{j}_{\max}^{[i]}(\sigma^\infty)$ predicted by the model, as it will be demonstrated in Section 3.4.

Equation 14 defines the expected level- $\hat{j}_{\max}^{[i]}$ of the largest broken-cluster in a level-[i] bundle. However, the surviving

level- $\hat{j}_{\max}^{[i]}$ sub-bundle ($\mathcal{B}^{[\hat{j}_{\max}^{[i]}]}$ in Fig. 2b) may still contain broken clusters of level- $[j' \leq \hat{j}_{\max}^{[i]} - 1]$, as discussed in Section 2.5.2. For this reason, the number of broken fibres in the largest cluster of level- $\hat{j}_{\max}^{[i]}$ can be any of the elements of the following set:

$$n_{\text{clust}}^{[j_{\max}^{[i]}]} = \left\{ 2^{\hat{j}_{\max}^{[i]}}, 2^{\hat{j}_{\max}^{[i]}} + 1, \dots, 2^{\hat{j}_{\max}^{[i]}+1} - 1 \right\}. \quad (15)$$

The first element of the set shown in Equation 15 ($2^{\hat{j}_{\max}^{[i]}}$) corresponds to the case when sub-bundle $\mathcal{B}^{[\hat{j}_{\max}^{[i]}]}$ is fully broken, but there is no single broken-fibre in its neighbour $\mathcal{B}^{[\hat{j}_{\max}^{[i]}]}$ (within the respective control length). The last element of the set ($2^{\hat{j}_{\max}^{[i]}+1} - 1$) corresponds to the case when the surviving $\mathcal{B}^{[\hat{j}_{\max}^{[i]}]}$ sub-bundle has only one unbroken fibre in the control length.

The critical broken-cluster ($\hat{j}_{\text{crit}}^{[i]}$) of a level- $[i]$ bundle is defined as the largest cluster predicted at the expected bundle strength ($\hat{X}^{[i]}$). Mathematically,

$$\begin{aligned} \hat{j}_{\text{crit}}^{[i]} &\stackrel{\text{def}}{=} \hat{j}_{\max}^{[i]} \left(\sigma^\infty \equiv \hat{X}^{[i]} \right), \quad \text{where} \\ \hat{X}^{[i]} &= \int_{\sigma^\infty=0}^{\infty} \sigma^\infty \cdot \frac{dF_{U,S}^{[i]}(\sigma^\infty)}{d\sigma^\infty} d\sigma^\infty. \end{aligned} \quad (16)$$

2.6. Model implementation

Fig. 3 shows an overview of the vectorial MATLAB® [42] implementation of the model described in this paper, which follows the same principles used previously for scaling the strength of composite fibre-bundles [32]. To avoid numerical errors due to very small values of survival probability terms, Equations 3, 5a, 5b and 9 are written in logarithmic form.

3. Results

3.1. Overview of model results

Fig. 4 gives an overview of the results of the model for the nominal inputs shown in Table 1 (which represent a carbon/epoxy system). The model predicts that individual fibres start breaking at relatively low values of the applied stress (see curve for $j = 0$ in Fig. 4c), and small broken-clusters progressively form with increasing applied load (Fig. 4d); this is in agreement with experimental observations [1,2].

At high applied stresses, the expected density of broken clusters starts decreasing, but (for reasonable bundle lengths) this occurs after the overall bundle is expected to fail: for instance, the expected number of level-[2] clusters starts decreasing for $\sigma^\infty \geq 5.4$ GPa ($j = 2$ in Fig. 4c), but level-[3] bundles (10 mm long) are expected to fail at a lower stress of 5.1 GPa (Fig. 4a). This means that the model predicts that the total density of fibre-breaks increases monotonically during the expected stress-strain curve; it also implies that exceptionally strong bundles (i.e. on the right tail of the strength distribution) necessarily experience less fibre-breakage along the full stress-strain curve than bundles with average strength.

A small degree of non-linearity is predicted for small bundles ($i \leq 5$ or $n^{[i]} \leq 32$ in Fig. 4b), due to the accumulation of fibre-breaks and small broken-clusters. However, the stress-strain response is

almost linear for larger bundles, which agrees with the (macroscopically) brittle failure typically reported for coupon-sized specimens under longitudinal tension [43,44].

3.2. Effect of micromechanical properties

Figs. 5a and 6a show that the tensile strength of composites can be increased by both (i) decreasing the single-fibre Weibull modulus m and (ii) increasing the matrix/interface shear-lag strength τ_{SL} . However, these two properties influence the accumulation of damage and material non-linearity very differently:

- (i) Decreasing m (or increasing the variability of fibre strength) promotes failure of individual fibres but delays the formation of large clusters (Fig. 5d). The correlation between (i) the density of fibre-breaks and (ii) the non-linearity at a given applied stress is evidenced in Fig. 5b–c, which shows that these two features are affected by m in very similar ways;
- (ii) Increasing τ_{SL} does not affect the onset of fibre breakage, but it delays the formation of larger clusters (Fig. 6d). The density of fibre-breaks at a given applied stress decreases slightly with increasing shear-strength (Fig. 6c), but the non-linearity decreases significantly (Fig. 6d) due to reduced density of clusters formed.

This suggests that individual fibre-breaks dominate the damage accumulation in composite bundles, but the non-linearity at a given applied stress is dominated by the formation of clusters of broken fibres.

3.3. Size effects on the accumulation and clustering of fibre breaks

Fig. 7 shows the effect of specimen size on the accumulation of damage. Longer specimens are more likely to have weaker elements and, consequently, are expected to experience the first fibre-breaks and broken-clusters at lower stresses than shorter specimens (as shown in Fig. 7a). While the density of fibre-breaks and broken-clusters at a given remote stress is mathematically independent of the bundle length, it increases with the bundle level i or filament count $n^{[i]}$ (see Equation 10); this increase is only noticeable for bundles with very few fibres (e.g. below level [3] in Fig. 7b), as the contribution from larger broken-clusters (which would be allowed to form only in even larger bundles) becomes negligible.

Fig. 7c would appear to suggest that the size of the critical broken-cluster (which triggers failure of the entire specimen) stabilises at 16–32 fibres for large bundles. However, Fig. 7d (which considers a larger range of filament counts n^f in a logarithmic scale) shows that the critical cluster size actually keeps on increasing (albeit at a slowing rate) as the filament count increases further.

3.4. Experimental validation

Fig. 8 compares predictions of the model for the accumulation and clustering of fibre-breaks against experimental results obtained by Scott et al. [2,37] through in-situ high-resolution CT of one carbon-epoxy (T700/M21) specimen. The model requires micromechanical properties which are recognizably difficult to measure [26,45]; for that reason, four different datasets of inputs for the T700/M21 system were collected from the literature [2,31,46–48], as shown in Table 2.

In the experiments, a broken-cluster with n_{clust} fibres was defined as a group of n_{clust} adjacent fibre-breaks within an axial

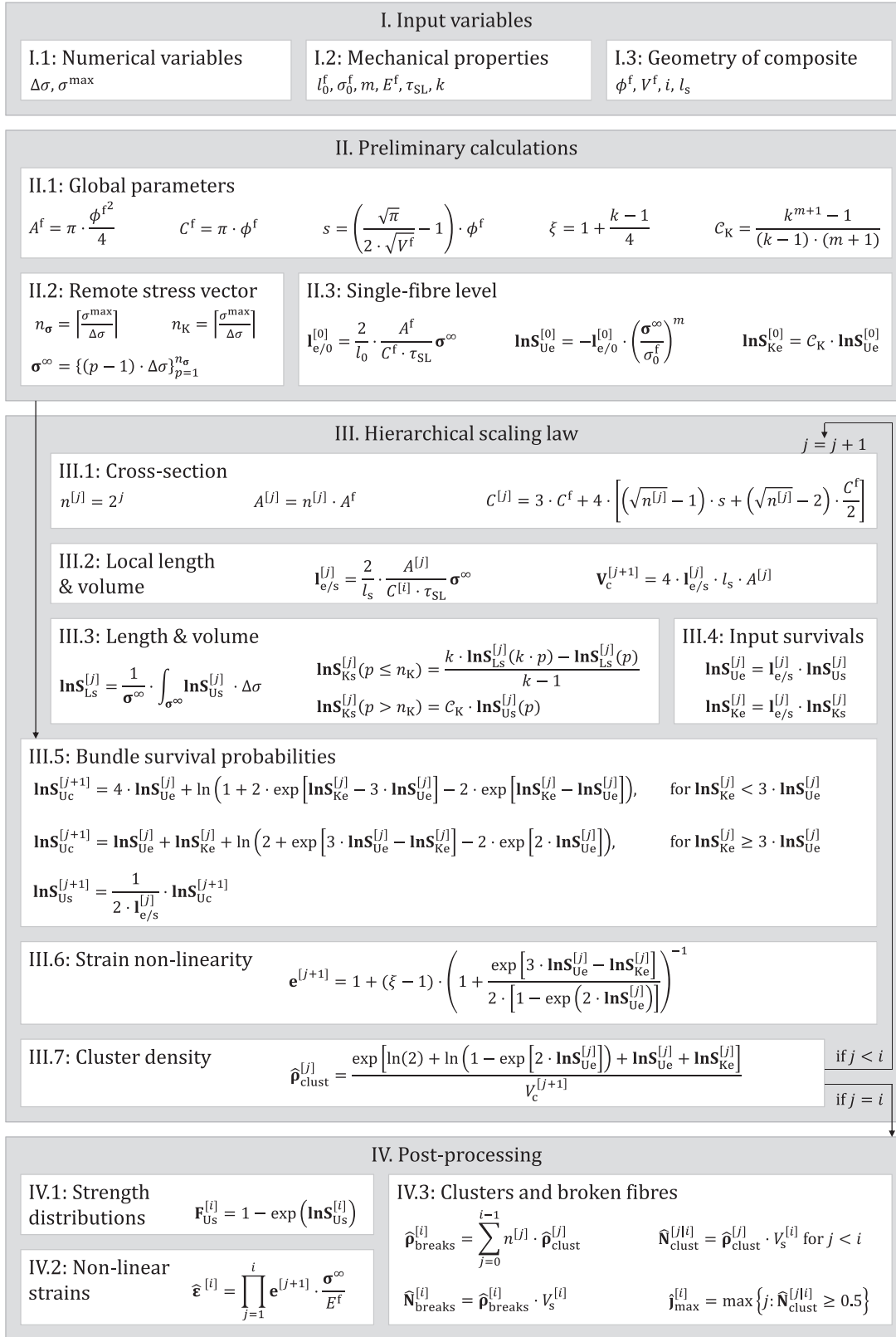


Fig. 3. Implementation of the hierarchical scaling law for calculating the strength, non-linear stress-strain response, and accumulation of fibre-breaks in a level-[i] composite fibre-bundle. All arithmetic operators represent pointwise calculations.

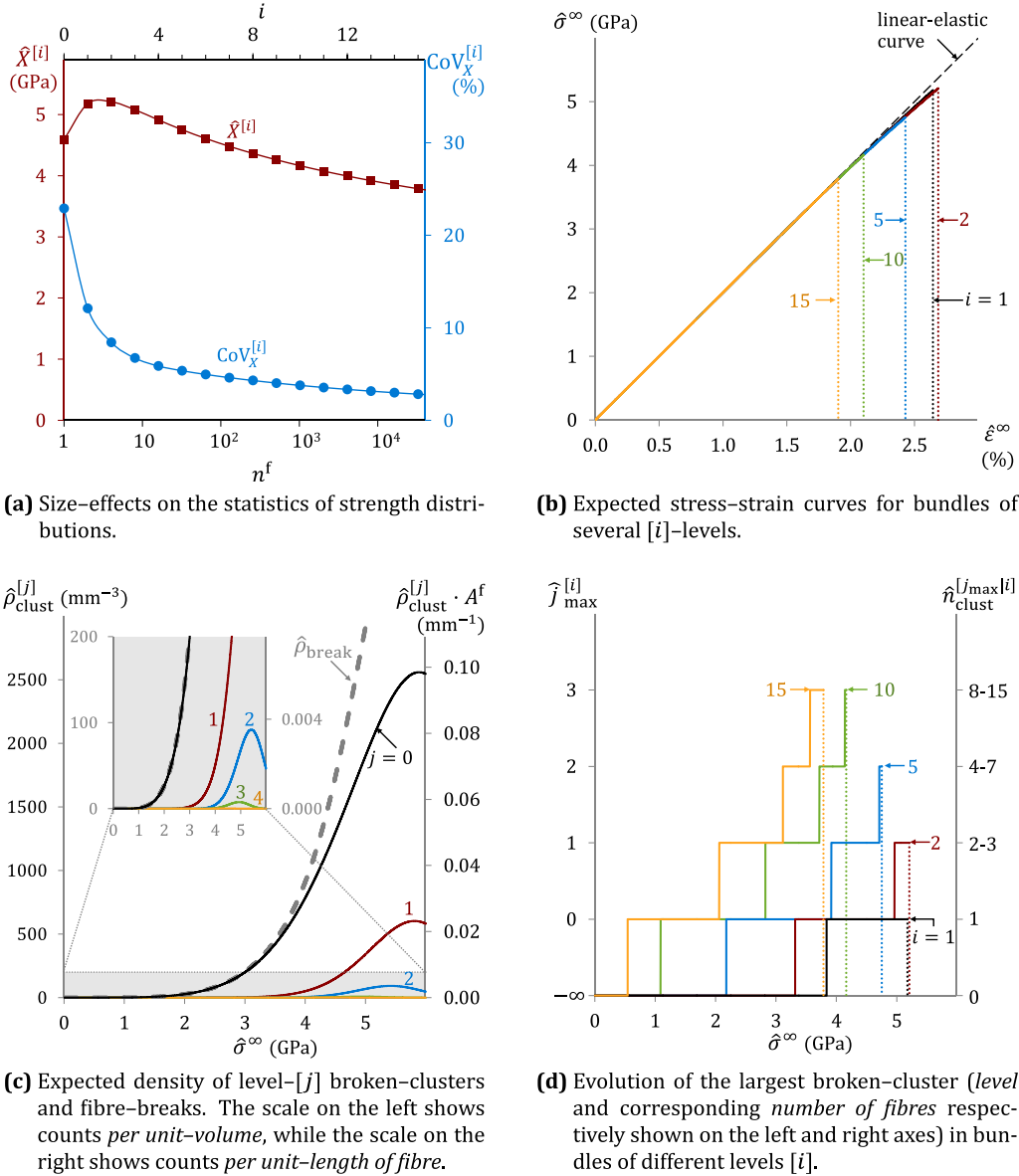


Fig. 4. Overview of model outputs for the nominal configuration (Table 1).

distance smaller than $70 \mu\text{m}$ [2,37]; this definition is different from that used in the model (in which clusters are defined as fibre-breaks within the same sub-bundle and within an axial distance equal to the control length, see Equation 4). Nevertheless, because approximately 70% of the clusters observed experimentally were co-planar [31], it is unlikely that changing the definition of a cluster in the experiments would change significantly the results shown in Fig. 8.

A good agreement between modelling and experimental results for the progressive accumulation of fibre-breaks is found (Fig. 8a), although the model seems to slightly underpredict the formation of large broken-clusters in favour of individual-fibre breaks. Regarding the size of the largest broken-cluster in the specimen (Fig. 8b), it must be noted that, just before failure, the model predicts a number $\hat{N}_{\text{clust}}^{[3]} = 0.45$ of occurrences of level-[3] broken-clusters per specimen; this is just below the 0.5 threshold for

Table 1

Material properties used as nominal model inputs. The following numerical parameters were used: $\sigma_{\max} = 50 \text{ GPa}$, $\Delta\sigma = 1 \text{ MPa}$, $k = 2$.

Mechanical properties					Geometry		
$l_0^f(\text{mm})$	$\sigma_0^f(\text{GPa})$	$m(-)$	$E^f(\text{GPa})$	$\tau_{\text{SL}}(\text{MPa})$	$\phi^f(\mu\text{m})$	$V^f(\%)$	$l_s(\text{mm})$
10	5.0	5.0	200	70	7.0	50	10

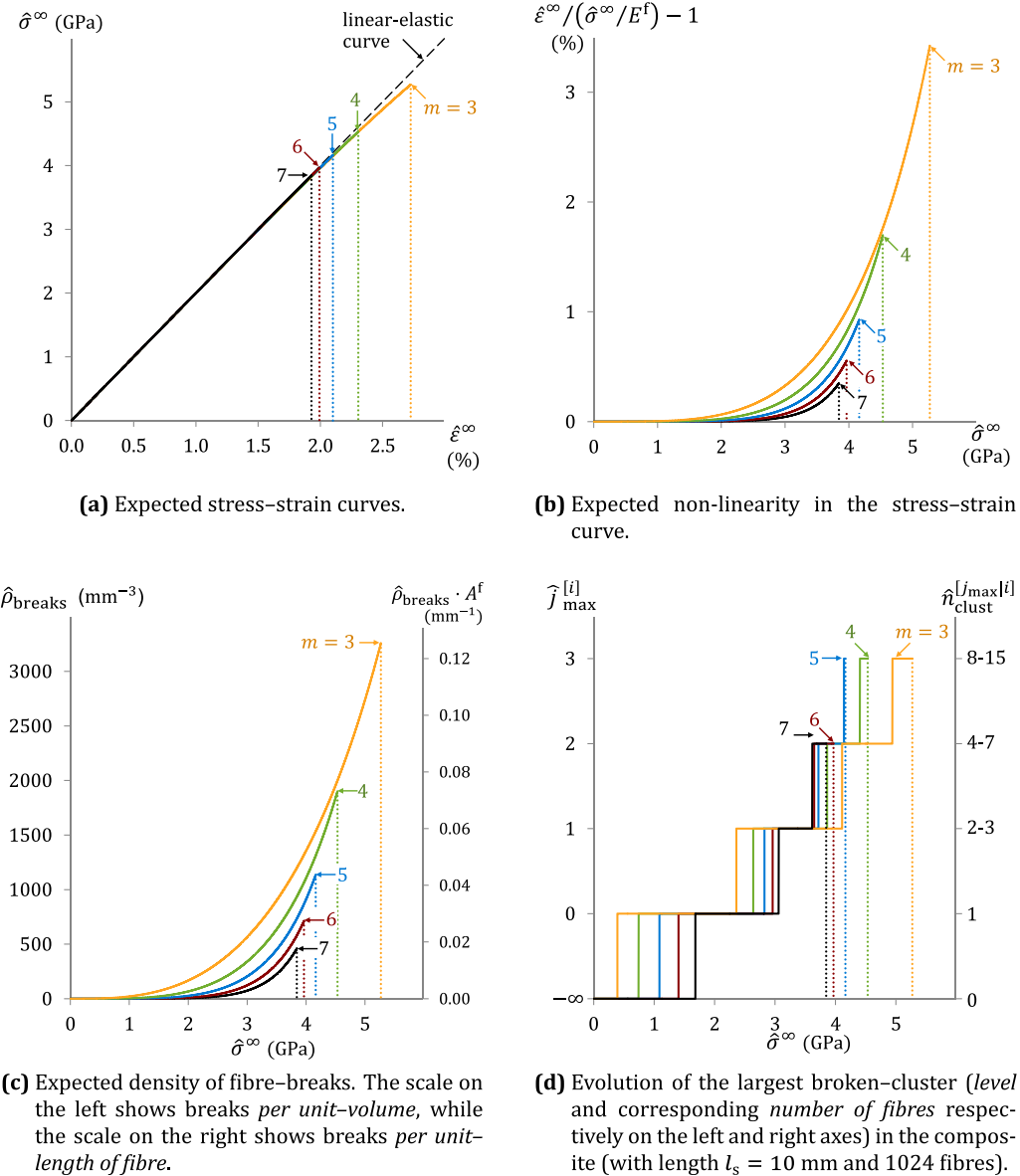


Fig. 5. Effect of the Weibull modulus m on the non-linearity and damage accumulation in composite fibre-bundles (all other inputs are shown in Table 1).

cluster detection (defined in Equation 14), meaning that the model is very close to predicting the formation of a cluster with 8–15 broken fibres. Fig. 8d also shows that the exact value of the threshold for detecting broken-clusters of a given size (nominally set as $N_{\text{thresh}} = 0.5$, see Section 2.5.3) does not affect the predictions of the model significantly (compare the ‘nominal’ (with $N_{\text{thresh}} = 0.5$) and ‘nominal, $N_{\text{thresh}} = 1$ ’ curves in Fig. 8d).

The predictions for the evolution of the number of fibre-breaks (in Fig. 8c) and for the size of the largest broken-cluster (in Fig. 8d) are not overly sensitive to the exact inputs of the model (within the reasonable values reported in Table 2). The most critical inputs for the results are the single-fibre strength parameters (m and σ_0^f), although their effect is much more pronounced on the final strength than on the accumulation of damage.

4. Discussion

4.1. Insight on the response of unidirectional composites under longitudinal tension

The model proposed in this paper provides the following insight on the tensile response and failure process of composite fibre-bundles:

- The overall density of fibre-breaks is dominated by uncorrelated failure of individual fibres (Figs. 4c and 8a), and is therefore governed by the variability of fibre-strength (see considerable effect of m in Fig. 5c). Consequently, the model predicts that the density of fibre-breaks is nearly not affected by the stress-transfer from broken-fibres (see

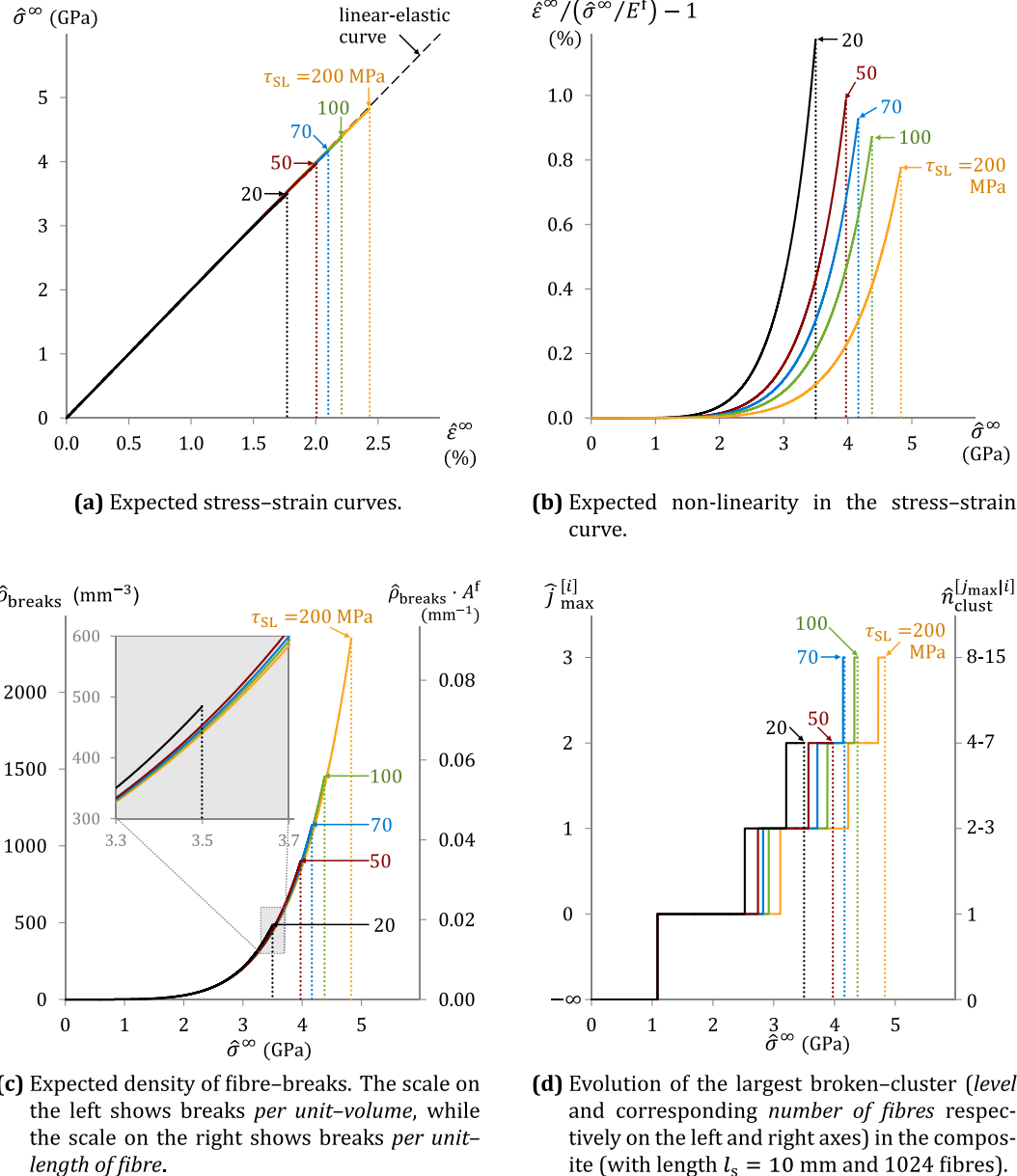


Fig. 6. Effect of the shear-lag strength τ_{SL} on the non-linearity and damage accumulation in composite fibre-bundles (all other inputs are shown in Table 1).

- negligible effect of τ_{SL} in Fig. 6c); however, this can be investigated further with more realistic stress-concentration fields (which were simplified to $k=2$ at the nearest-neighbour in the present model);
- (b) The formation of clusters of broken-fibres is governed by (i) the stress-transfer near fibre-breaks (see effect of τ_{SL} in Fig. 6d), and (ii) a stochastic process (see effect of strength variability in Fig. 5d, and of the specimen size both in terms of filament count and specimen length in Figs. 4d and 7);
 - (c) The evolution of individual fibre-breaks or small broken-clusters (with $j \leq 1$ and 1–3 fibre-breaks) has no correlation with the ultimate strength of the specimen (see Figs. 6c, 7b and 8c). However, there is a strong correlation between (i) delaying the formation of medium-sized clusters (with $j \leq 3$

or 4–7 fibre-breaks) and (ii) achieving high strength (see Figs. 4d, 5d, 6d, 7a and 8d);

- (d) The critical size of a broken cluster increases steadily with the size of the structure (as shown in Fig. 7a and d). This effect has been explicitly studied by only a few models in the literature [18,26], which either have considered small bundles only [26], or have not been applied to a real composite or representative case [18]. The results shown in Fig. 7d therefore demonstrate that calculating the critical cluster size based on expressions which do not account for the size of the structure [5,22] should be avoided. This also implies that the WLT can be used to scale the results of small-bundle simulations to large structures only within a limited range of sizes, because the size of the *independent link* (which is

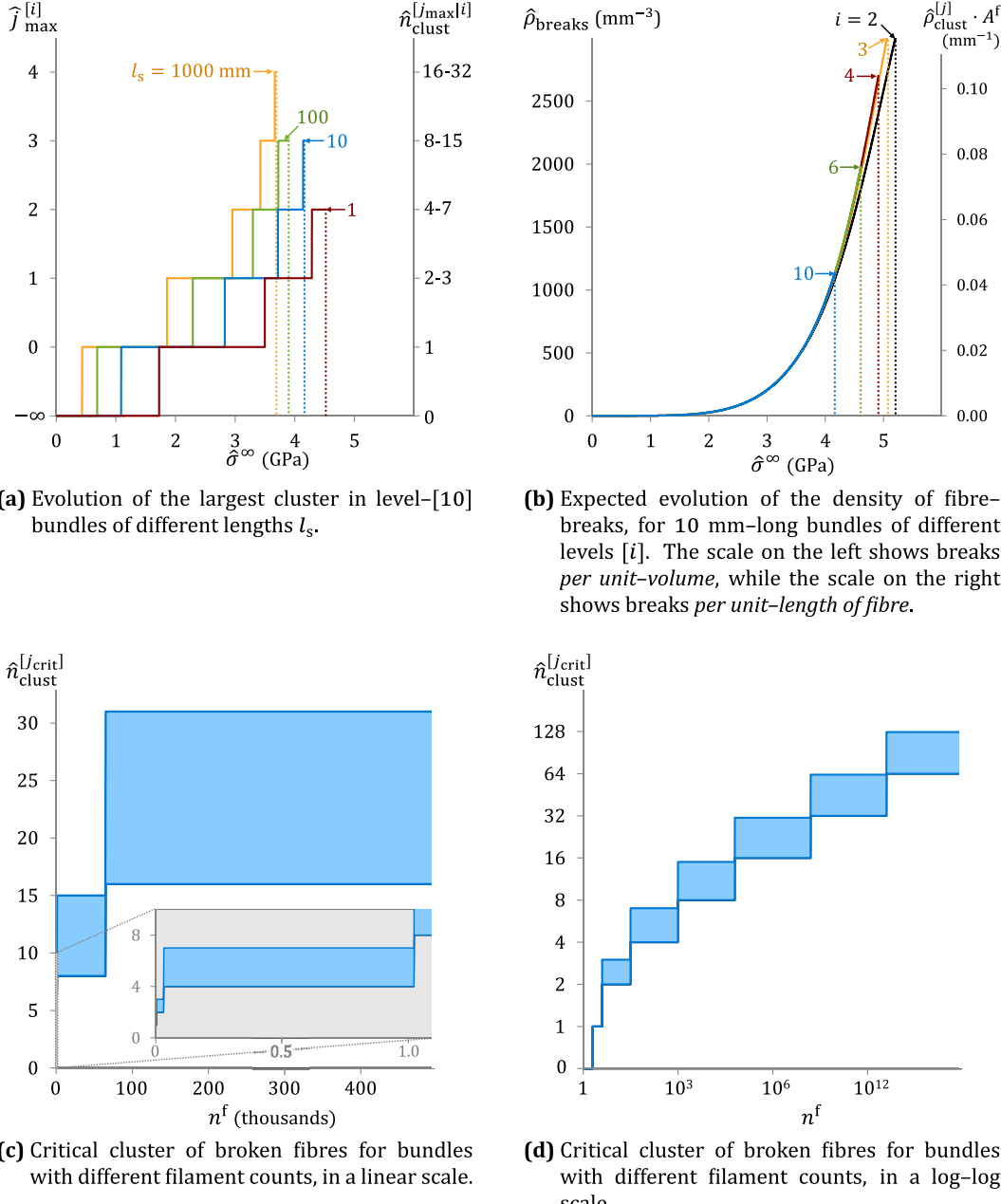


Fig. 7. Effect of specimen size on the accumulation and clustering of fibre-breaks.

necessarily related to the critical cluster size) increases with the overall size of the structure (meaning that one would need progressively larger simulated volumes before applying the WLT);

- (e) Composite fibre-bundles under longitudinal tension present a negligible amount of non-linearity because (i) they accumulate damage mostly as individual fibre-breaks (see Figs. 4c and 8a), which increase the compliance of the material very locally only, and (ii) they fail prematurely (see small non-linearity predicted for level-[1] and level-[2] bundles in Fig. 4b, which also have the highest strength as shown in Fig. 4a). Promoting the clustering of broken-fibres (which increases the compliance in a larger volume than individual fibre-breaks) would increase the non-linearity of

the material at a given remote stress (as shown when reducing τ_{SL} in Fig. 6); in order to maximise non-linearity, this should be achieved without weakening the material, although these two objectives are (as discussed in point (c)) difficult to conciliate.

4.2. Comparison between model predictions and experimental data

In a nutshell, the model proposed in this paper predicts that individual fibre-breaks start accumulating at very low applied stresses, due to variability of fibre strength; although clusters are formed and accumulate as the remote load increases, most fibre-breaks are isolated and uncorrelated, and they have nearly no

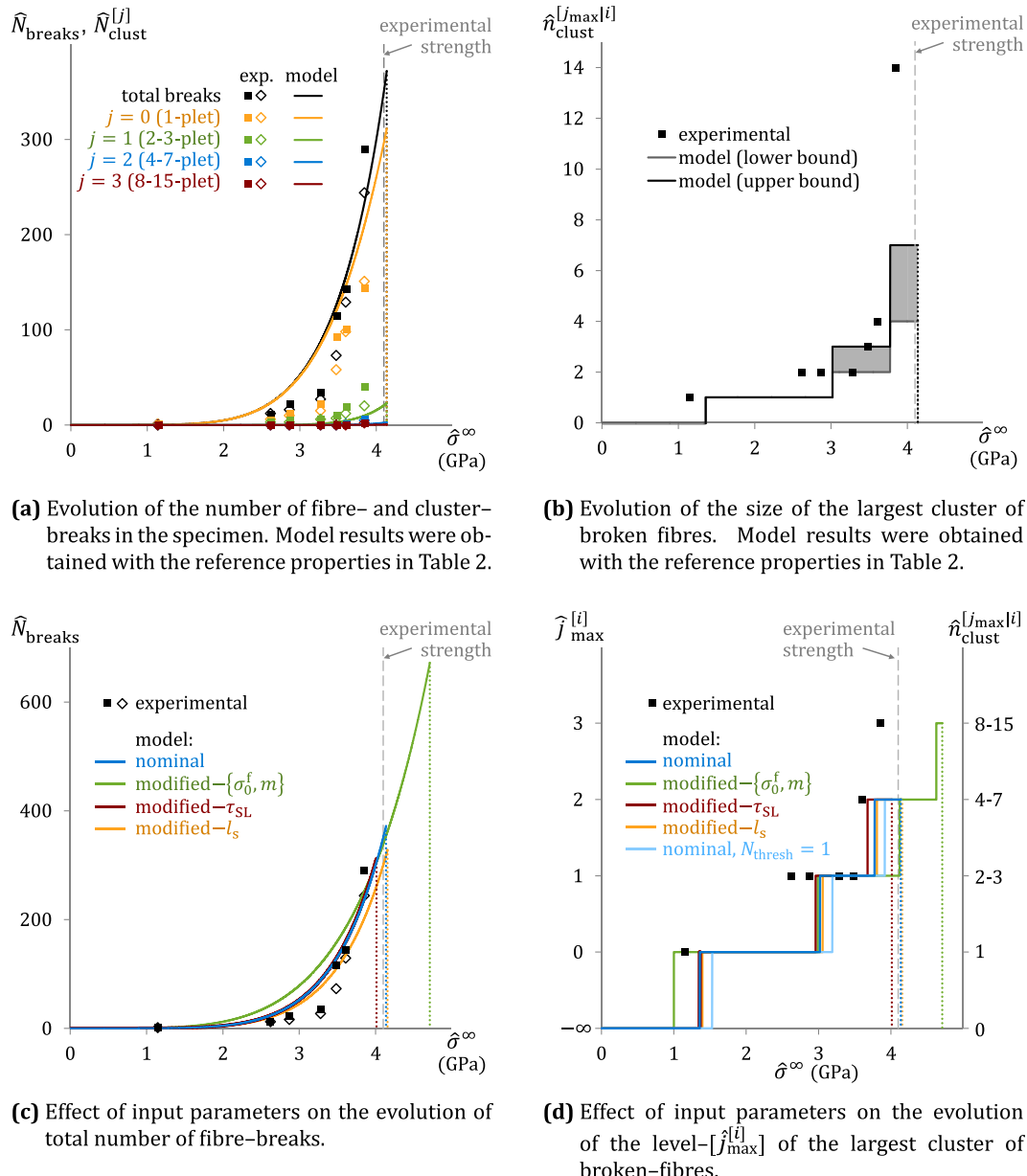


Fig. 8. Comparison between experimental results (from Scott et al. [2,37]) and model predictions. Subfigures (a) and (c) include two (slightly different, but obtained with the same specimen) experimental datasets published by Scott et al. in 2011 (shown as ■ [2]) and in 2012 (shown as ◇ [37]); the largest clusters reported by Scott et al. in both publications [2,37] were coincident, hence only one experimental dataset is explicitly shown in subfigures (b) and (d). The threshold for detecting the formation of clusters was set to its nominal value $N_{\text{thresh}} = 0.5$ (see Section 2.5.3) in all cases, except for one curve ('nominal, $N_{\text{thresh}} = 1$ ') in subfigure (d).

Table 2

Datasets of properties for the T700/M21 system tested by Scott et al. [2], used for experimental validation. For the 'modified' datasets, only the modified parameters are mentioned (all others remain equal to the 'nominal' dataset). The following numerical parameters were used in all cases: $\sigma_{\text{max}} = 50$ GPa, $\Delta\sigma = 1$ MPa, $k = 2$.

Dataset	Mechanical properties				Geometry			
	l_0^f (mm)	σ_0^f (GPa)	m (–)	τ_{SL} (MPa)	ϕ^f (μm)	V^f (%)	l_s (mm)	n_s^f (–)
nominal	1.0 ^a	7.338 ^a	5.86 ^a	105 ^b	7.1 ^a	60 ^c	1.8 ^c	5444 ^c
modified- $\{\sigma_0^f, m\}$	10 ^d	5.2 ^d	4.6 ^d		81.2 ^e			
modified- τ_{SL}								
modified- l_s								1.54 ^f

^a T700G fibre properties measured through SFTT (parameters estimated from at least 75 samples tested over three gauge lengths) [46].

^b Interlaminar shear strength for the T700G/M21 system (fibre areal weight: 268 g/m²) [48].

^c CT-specimen geometry as reported by Scott et al. [2].

^d T700S fibre properties measured through SFTT (parameters estimated from at least 100 samples tested at 10 mm) [47].

^e Interfacial shear strength for T700S/Araldite-F (sized), measured through single-fibre pull-out tests [48].

^f Updated length of the CT-specimen where fibre-breaks were observed [31].

effect on the overall macroscopic response of the material. This correlates very well with experimental results from the literature [1,2], as shown in Fig. 8.

The good agreement between model predictions and experimental data [2] for the accumulation and clustering of fibre-breaks (Fig. 8a–b) is encouraging. The model overpredicts slightly the formation of individual fibre-breaks at intermediate stresses (2.5–3.5 GPa), and underpredicts the formation of broken-clusters throughout the analysis; this could be due to the simplifications assumed in the model, or to inherent variability in the experimental results (as the experimental data corresponds to one single sample) [2,37].

The dataset used for experimental validation in this work had already been compared against results from two other models in the literature [31,37], both based on computationally-expensive Monte-Carlo analyses involving FE simulations. Still, the correlation between predictions of the present model and micro-CT experimental results (Fig. 8) is actually better than that previously obtained with those models [31,37]. While the uncertainty associated with input properties and experimental variability hinders a conclusive comparison, this shows that the model assumptions described in Section 2.1 are suitable to represent the micro-mechanics of longitudinal tensile failure in UD-FRPs in a computationally efficient way.

4.3. Analysis of the model in the scope of the literature

Compared to other fibre-bundle models from the literature, the one proposed in this paper presents the following features:

- (a) *Computational efficiency and ability to cope with large composite fibre-bundles.* The present model is analytical and, consequently, calculates the expected stress-strain curves and the evolution of fibre-breaks and clusters in less than one second, even for bundles with a trillion fibres. On the contrary, most state-of-the-art literature models [5,16–27,30] (which require Monte-Carlo and/or Finite Element simulations) are computationally much more demanding, which limits the maximum size of the structures that they can analyse. This is particularly important given the results showing an increasing critical cluster size for larger structures (point (d) in Section 4.1), which limit the applicability of the WLT to scale-up results from simulations of small bundles;
- (b) *Ability to predict stress-strain curves accurately.* The present model predicts quasi-linear stress-strain responses for composite fibre-bundles with reasonable size and micro-mechanical properties (Fig. 4b), which agrees with experimental observations of macroscopically brittle failure in UD composites [43,44]. On the contrary, most literature models have either (i) not predicted stress-strain curves (as it is the case for most analytical approaches [12–19]), or (ii) predict significant non-linearities before failure [5,20,22,23,25,27];
- (c) *Ability to predict the correct level of fibre breakage and clustering.* It is predicted that, for average-sized structures, the material should withstand clusters with 8–32 broken fibres before catastrophic failure (Fig. 7c). Other models in the literature tend to predict larger amounts of fibre breakage [18–21,23–27,31] and larger critical cluster sizes [5,18–21,23–27]. However, the predictions from the present model were actually validated quantitatively against experiments [2], which is only the case for very few literature models [31,37]; this increases the confidence on the results obtained with the present model.

The hierarchical scaling law presents the following advantages compared to literature analytical models:

- (i) It considers *varying stress concentrations in the recovery length* of surviving fibres, rather than simply assuming that the entire recovery length experiences the maximum stress concentration [5,12–19];
- (ii) It considers *matrix plasticity*, rather than assuming a linear-elastic constitutive law [5,12,14–19].
- (iii) It calculates strength distributions, accumulation of fibre breaks, size effects on strength and critical cluster size, and full stress-strain curves, and is *validated against experiments* in all of those aspects.

The hierarchical scaling law proposed in this work differs from computationally-intensive Monte-Carlo simulations [5,16–27,31] in five aspects:

- (i) The present model assumes that *clusters are co-planar and grow in discrete steps*, contrasting with the progressive growth of diffuse clusters predicted in most literature simulations [17,19–26,31]. Nevertheless, experimental data [31,35,39,40] supports this assumption in the present model;
- (ii) The model assumptions (Section 2.1) lead to a *stress concentration factor k = 2*, which is higher than that calculated through FE analyses [8,11,24,41] and could potentially lead to underpredicted composite strengths. Nevertheless, this may actually indirectly account for some of the features of actual composites which may reduce their strength (e.g. dynamic effects, fibre misalignments, and large broken clusters) and which are presently missing in most literature models [5,16–27];
- (iii) The present model uses a *constant shear-lag stress τ_{SL}* , which can represent either a perfectly-plastic matrix/interface, or a debonded interface with uniform friction. Other Monte-Carlo simulations have considered other matrix and/or interface responses, e.g. with viscoelasticity [27], strain-hardening [23,24,29], transverse matrix cracks [29], progressive decohesion [29], or with a given debond length [27]. However, the impact of considering more complex matrix/interface constitutive laws on the predicted strength and fibre-damage accumulation in composites is still to be quantified;
- (iv) The present model can be used to *model UD-FRPs of any size*, and it suggests that the critical cluster becomes larger for larger structures; on the contrary, it is often assumed in the literature that the critical cluster size does not depend on the specimen size [21,22]. This implies that the WLT may not be used to extrapolate the results of small-scale simulations to very large bundles, since the size of independent links actually depends on the size of the structure.
- (v) The present formulation can be *used not only by modellers, but also by experimentalists or material developers* without expertise in numerical methods, whom may simply introduce the relevant inputs and run the model to explain the results of their experiments or to perform parametric studies, in a simple and time-efficient way.

5. Conclusions

This paper proposed an analytical model to predict progressive fibre-breakage and the stress/strain response of composite fibre-bundles under longitudinal tension. The following conclusions were reached:

- The model is based on a hierarchical scaling law [32] and considers the statistics of fibre–strength and a shear–lag stress–transfer near fibre–breaks *analytically*. This makes the model capable of calculating composite bundles with virtually any number of fibres in less than one second;
- Model predictions reproduce experimental results from in-situ computed tomography [2], making this model an accurate alternative to much more computationally-expensive simulations in the literature;
- The model shows that the reduced number and size of broken-fibre clusters and the premature failure of large specimens hinder any noticeable non-linearity in macroscopic stress-strain curves;
- The model suggests that there is no universal size for the critical cluster; this implies that the weakest-link theory cannot be used to scale-up the results of small-bundle simulations to very large structures, because the size of independent material links actually increases with the overall size of the structure.

Acknowledgements

S. Pimenta acknowledges the the Royal Academy of Engineering for her Research Fellowship on *Multiscale discontinuous composites for large scale and sustainable structural applications* (2015–2019). This work was also done in the scope of the UK EPSRC Programme Grant EP/I02946X/1 on *High Performance Ductile Composite Technology* in collaboration with the University of Bristol.

The author acknowledges Hannah Morton from the University of Southampton and Serafina Garcea from the University of Manchester for discussions on the high-resolution computed tomography experiments.

Supporting data and the MATLAB® implementation can be requested from the corresponding author.

Appendix A. Geometry of the cross-section of a composite fibre-bundle

For a level-[i] bundle (with $n^{[i]}$ fibres, fibre diameter ϕ^f , and fibre volume fraction V^f), the cross-sectional area $A^{[i]}$ (based on the fibres only) is

$$A^{[i]} = n^{[i]} \cdot A^f, \quad \text{with} \quad A^f = \pi \cdot \frac{(\phi^f)^2}{4}.$$

Assuming a square fibre-packing and preferential interfacial failure (see Fig. 1b), the level-[i] shear-lag perimeter is:

$$\begin{aligned} C^{[i]} &= 3 \cdot C^f + 4 \cdot \left[(\sqrt{n^{[i]}} - 1) \cdot s + (\sqrt{n^{[i]}} - 2) \cdot \frac{C^f}{2} \right], \quad \text{with} \\ C^f &= \pi \cdot \phi^f \quad \text{and} \quad s = \left(\frac{\sqrt{\pi}}{2 \cdot \sqrt{V^f}} - 1 \right) \cdot \phi^f. \end{aligned}$$

Appendix B. Definition of the survival probability terms required for the scaling law

Equation 3 defines a hierarchical scaling law relating the survival probability $S_{U,c}^{[i+1]}(\sigma^\infty)$ of a level-[i+1] bundle under uniform stresses in its control length ($l_c^{[i+1]}$, see Equation 4) to the survival probabilities of a level-[i] sub-bundle in its recovery length ($l_e^{[i]}$, see

Equation 4), either under an uniform stress ($S_{U,e}^{[i]}(\sigma^\infty)$) or under linear stress concentrations ($S_{K,e}^{[i]}(\sigma^\infty; k=2)$). While full derivations can be found elsewhere [32], these terms can be calculated as:

- For $i=0$, assuming the single-fibre strength distribution defined in Equation 2:

$$S_{U,e}^{[0]}(\sigma^\infty) = \exp \left[- \frac{l_e^{[0]}}{l_0} \cdot \left(\frac{\sigma^\infty}{\sigma_0^f} \right)^m \right],$$

$$S_{K,e}^{[0]}(\sigma^\infty) = \exp \left[- \mathcal{C}_K \cdot \frac{l_e^{[0]}}{l_0} \cdot \left(\frac{\sigma^\infty}{\sigma_0^f} \right)^m \right], \quad \text{with} \\ \mathcal{C}_K = \frac{k^{m+1} - 1}{(m+1) \cdot (k-1)}.$$

- For $i \geq 1$, assuming that $S_{U,c}^{[i]}(\sigma^\infty)$ has been calculated through the scaling law (Equation 3):

$$\ln \left[S_{U,e}^{[i]}(\sigma^\infty) \right] = \frac{l_e^{[i]}}{l_c^{[i]}} \cdot \ln \left[S_{U,c}^{[i]}(\sigma^\infty) \right],$$

$$\ln \left[S_{K,s}^{[i]}(\sigma^\infty) \right] = \frac{k \cdot \ln \left[S_{L,s}^{[i]}(k \cdot \sigma^\infty) \right] - \ln \left[S_{L,s}^{[i]}(\sigma^\infty) \right]}{k-1}, \quad \text{with}$$

$$\ln \left[S_{L,s}^{[i]}(\sigma) \right] = \frac{1}{\sigma} \int_{\sigma_L=0}^{\sigma} \ln \left[S_{U,s}^{[i]}(\sigma_L) \right] d\sigma_L.$$

References

- [1] D.R.B. Aroush, et al., A study of fracture of unidirectional composites using in situ high-resolution synchrotron X-ray microtomography, Compos Sci. Technol. 66 (2006) 1348–1353.
- [2] A.E. Scott, et al., In situ fibre fracture measurement in carbon-epoxy laminates using high resolution computed tomography, Compos Sci. Technol. 71 (2011) 1471–1477.
- [3] G.W. Weibull, A statistical distribution function of wide applicability, J. Appl. Math. 18 (1951) 293–297.
- [4] J. Watanabe, et al., Tensile strength distribution of carbon fibers at short gauge lengths, Adv. Compos Mater 23 (2014) 535–550.
- [5] W.A. Curtin, Tensile strength of fiber-reinforced composites: III. Beyond the traditional Weibull model for fiber strengths, J. Compos Mater 34 (2000) 1301–1332.
- [6] E.G. Stoner, et al., An end-effect model for the single-filament tensile test, J. Mater Sci. 29 (1994) 6561–6574.
- [7] J.L. Thomason, On the application of Weibull analysis to experimentally determined single fibre strength distributions, Compos Sci. Technol. 77 (2013) 74–80.
- [8] Y. Swolfs, et al., Stress concentrations in an impregnated fibre bundle with random fibre packing, Compos Sci. Technol. 74 (2013) 113–120.
- [9] I.J. Beyerlein, S.L. Phoenix, Stress concentrations around multiple fiber breaks in an elastic matrix with local yielding or debonding using quadratic influence superposition, J. Mech. Phys. Solids 44 (1996) 1997–2039.
- [10] J.A. Nairn, A variational mechanics analysis of the stresses around breaks in embedded fibers, Mech. Mater. 13 (1992) 131–154.
- [11] M.L. Accorsi, et al., Dynamic analysis of fibre breakage in single- and multiple-fibre composites, J. Mater Sci. 31 (1996) 4181–4187.
- [12] B.W. Rosen, Tensile failure of fibrous composites, AIAA J. 2 (1964) 1985–1991.
- [13] D.G. Harlow, S.L. Phoenix, The chain-of-bundles probability model for the strength of fibrous materials I: analysis and conjectures, J. Compos Mater 12 (1978) 195–214.
- [14] S.L. Phoenix, R.L. Smith, A comparison of probabilistic techniques for the strength of fibrous materials under local load-sharing among fibers, Int. J. Solid Struct. 19 (1983) 479–496.
- [15] W.A. Curtin, Theory of mechanical properties of ceramic–matrix composites, J. Am. Ceram. Soc. 74 (1991) 2837–2845.
- [16] S.L. Phoenix, et al., Size effects in the distribution for strength of brittle matrix fibrous composites, Int. J. Solid Struct. 34 (1997) 545–568.

- [17] W.A. Curtin, Size scaling of strength in heterogeneous materials, *Phys. Rev. Lett.* 80 (1997) 1445–1448.
- [18] S. Mahesh, et al., Strength distributions and size effects for 2D and 3D composites with Weibull fibers in an elastic matrix, *Int. J. Fract.* 115 (2002) 41–85.
- [19] C. Habeeb, S. Mahesh, Strength distribution of planar local load-sharing bundles, *Phys. Rev. E* 92 (022125) (2015).
- [20] S.J. Zhou, W.A. Curtin, Failure of fiber composites: a lattice green function model, *Acta Metall. Mater.* 43 (1994) 3093–3104.
- [21] M. Ibnabdeljalil, W.A. Curtin, Strength and reliability of fiber-reinforced composites: localized load-sharing and associated size effects, *Int. J. Solid Struct.* 34 (1997) 2649–2668.
- [22] T. Okabe, N. Takeda, Size effect on tensile strength of unidirectional CFRP composites — experiment and simulation, *Compos Sci. Technol.* 62 (2002) 2053–2064.
- [23] T. Okabe, et al., Numerical method for failure simulation of unidirectional fiber-reinforced composites with spring element model, *Compos Sci. Technol.* 65 (2005) 921–933.
- [24] T. Okabe, et al., Prediction of tensile strength of unidirectional CFRP composites, *Adv. Compos Mater.* 19 (2010) 229–241.
- [25] C.M. Landis, et al., Micromechanical simulation of the failure of fiber reinforced composites, *J. Mech. Phys. Solids* 48 (2000) 621–648.
- [26] Y. Swolfs, et al., Issues in strength models for unidirectional fibre-reinforced composites related to Weibull distributions, fibre packings and boundary effects, *Compos Sci. Technol.* 114 (2015) 42–49.
- [27] S. Blassiau, et al., Damage accumulation processes and life prediction in unidirectional composites, *P. Roy. Soc. A* 463 (2007) 1135–1152.
- [28] G. Dai, L. Mishnaevsky Jr., Fatigue of hybrid glass/carbon composites: 3D computational studies, *Compos Sci. Technol.* 94 (2014) 71–79.
- [29] R.P. Tavares, et al., Mechanics of hybrid polymer composites: analytical and computational study, *Comput. Mech.* 57 (2016) 405–421.
- [30] L. St-Pierre, et al., Stress redistribution around clusters of broken fibres in a composite, *Compos Struct.* 168 (2017) 226–233.
- [31] Y. Swolfs, et al., Synchrotron radiation computed tomography for experimental validation of a tensile strength model for unidirectional fibre-reinforced composites, *Compos Part A—Appl S* 77 (2015) 106–113.
- [32] S. Pimenta, S.T. Pinho, Hierarchical scaling law for the strength of composite fibre bundles, *J. Mech. Phys. Solids* 61 (2013).
- [33] M. Kazanci, Carbon fiber reinforced microcomposites in two different epoxies, *Polym. Test.* 23 (2004) 747–753.
- [34] I.J. Beyerlein, S.L. Phoenix, Statistics for the strength and size effects of microcomposites with four carbon fibers in epoxy resin, *Compos Sci. Technol.* 56 (1996) 75–92.
- [35] S. Pimenta, S.T. Pinho, An analytical model for the translaminar fracture toughness of fibre composites with stochastic quasi-fractal fracture surfaces, *J. Mech. Phys. Solids* 66 (2014).
- [36] G. Bullegas, et al., Engineering the translaminar fracture behaviour of thin-ply composites, *Compos Sci. Technol.* 131 (2016) 110–122.
- [37] A.E. Scott, et al., Damage accumulation in a carbon/epoxy composite: comparison between a multiscale model and computed tomography experimental results, *Compos Part A—Appl S* 43 (2012) 1514–1522.
- [38] M.R. Wisnom, et al., Size effects in unnotched tensile strength of unidirectional and quasi-isotropic carbon/epoxy composites, *Compos Struct.* 84 (2008) 21–28.
- [39] S.T. Pinho, et al., Fracture toughness of the tensile and compressive fibre failure modes in laminated composites, *Compos Sci. Technol.* 66 (2006) 2069–2079.
- [40] S. Pimenta, et al., Mechanical analysis and toughening mechanisms of a multiphase recycled CFRP, *Compos Sci. Technol.* 70 (2010) 1713–1725.
- [41] A.B. de Moraes, Stress distribution along broken fibres in polymer–matrix composites, *Compos Sci. Technol.* 61 (2001) 1517–1580.
- [42] MATLAB®, Version 8.5.0 (R2015a), The MathWorks Inc., United States, 2015.
- [43] M.R. Wisnom, Size effects in the testing of fibre-composite materials, *Compos Sci. Technol.* 59 (1999) 1937–1957.
- [44] S.R. Hallett, et al., An experimental and numerical investigation into the damage mechanisms in notched composites, *Compos Part A—Appl S* 40 (2009) 613–624.
- [45] T. Hobbebrunken, et al., Experimental determination of the true epoxy resin strength using micro-scaled specimens, *Compos Part A—Appl S* 38 (2007) 814–818.
- [46] S. Bai, et al., Improving the adhesion between carbon fibres and an elastomer matrix using an acrylonitrile containing atmospheric plasma treatment, *Compos Interface* 20 (2013) 761–782.
- [47] J. Watanabe, et al., The tensile strength distribution of carbon fibers at short gauge length, in: 38th JSCM Domestic Symposium on Composite Materials, Kagoshima, Japan, 24–26, JSCM, September 2013.
- [48] Hexcel Corporation. HexPly M21 Product Data — Publication FTA 002c, March 2007.